water

MDPI

Article

CMADS and CFSR Data-Driven SWAT Modeling for Impacts of Climate and Land-Use Change on Runoff

Bailin Du [1,2], Lei Wu [1,2,3,*], Bingnan Ruan [1,2], Liujia Xu [1,2] and Shuai Liu [1,2]

[1] Key Laboratory of Agricultural Soil and Water Engineering in Arid and Semiarid Areas, Ministry of Education, Northwest A&F University, Yangling, Xianyang 712100, China; linshowing@nwafu.edu.cn (B.D.); rbn@nwafu.edu.cn (B.R.); xlj19980129@nwafu.edu.cn (L.X.); liushuai19990223@163.com (S.L.)

[2] College of Water Resources and Architectural Engineering, Northwest A&F University, Yangling, Xianyang 712100, China

[3] State Key Laboratory of Soil Erosion and Dryland Farming on the Loess Plateau, Northwest A&F University, Yangling, Xianyang 712100, China

* Correspondence: lwu@nwsuaf.edu.cn; Tel.: +86-158-2925-2152

Abstract: Climate and land-use change significantly impact hydrological processes and water resources management. However, studies of runoff simulation accuracy and attribution analysis in large-scale basins based on multi-source data and different scenario projections are limited. This study employed the Soil and Water Assessment Tool (SWAT) model in conjunction with spatial interpolation techniques to evaluate the accuracy of Climate Forecast System Reanalysis (CFSR), China Meteorological Assimilation Driven Dataset (CMADS), and observation (OBS) in runoff simulations, and configured various scenarios using the Patch-generating Land-use Simulation (PLUS) model to analyze effects of climate and land-use changes on runoff in the Jing River Basin from 1999 to 2018. Results demonstrated the superior performance of the CMADS+SWAT model compared to than CFSR+SWAT model, as the latter underestimated peak runoff. Changes in precipitation had a stronger impact on runoff than temperature, with increased flow from farmland and strong interception effects from forestland. Integrated climate and land-use changes led to an average annual runoff reduction of 1.24 m^3/s (I_2), primarily attributed to climate change (1.12 m^3/s, I_3), with a small contribution from land-use change (0.12 m^3/s, I_4). CMADS exhibited robust applicability under diverse scenarios, effectively enhancing runoff simulation accuracy. The findings provide invaluable guidance for water resources management in semi-arid regions.

Keywords: data precision; SWAT; scenario simulation; attribution analysis; runoff response

Citation: Du, B.; Wu, L.; Ruan, B.; Xu, L.; Liu, S. CMADS and CFSR Data-Driven SWAT Modeling for Impacts of Climate and Land-Use Change on Runoff. *Water* **2023**, *15*, 3240. https://doi.org/10.3390/w15183240

Academic Editor: Aizhong Ye

Received: 18 August 2023
Revised: 4 September 2023
Accepted: 8 September 2023
Published: 12 September 2023

1. Introduction

Climate and land-use changes have varying impacts on the hydrological cycle processes in watersheds, particularly leading to the significant spatiotemporal changes in runoff [1–3]. Climate change has a relatively long impact on runoff, primarily through direct effects of precipitation and indirect effects of temperature and evaporation [4,5], while land-use change has a relatively short impact, mainly affecting runoff through alterations in hydrological elements such as surface vegetation retention, infiltration, evaporation, and puddle filling [3,6]. With the effects of integrated climate and land-use change on runoff, runoff can either increase or decrease simultaneously, or display opposite trends with one factor increasing while the other decreases [7]. Runoff is a crucial foundation for the sustainable and healthy development of human society and ecosystems. However, quantifying the effects of climate and land-use changes on runoff in a scientific manner remains a challenging task for current research [8–11]. Commonly used quantification methods include empirical approaches [12], statistical methods [13], and hydrological modeling methods [14]. However, due to the complex interactions between climate and

land-use changes and their impacts on runoff variability and subsurface conditions, inconsistent results are obtained from different quantification methods [15]. Therefore, accurately simulating runoff processes in watersheds is of great significance in assessing the effects of climate and land-use changes and developing effective precautionary measures.

Meteorological data are crucial for accurately simulating hydrological processes and serve as an important indicator of climate change [16,17]. Precise hydrological simulation relies on reliable meteorological conditions [18,19]. Meteorological data are primarily obtained from gauged stations. However, there are challenges in obtaining meteorological data in areas with complex terrain due to scarcity and uneven spatial distribution of stations, limited time scales, and difficulties in data acquisition [20], which greatly restrict the accuracy requirement on hydrological modeling [21]. The use of reanalysis meteorological products is a reliable approach to address this issue and provide data support for hydrological analysis in data-scarce basins [22,23]. Compared to other reanalysis datasets, Climate Forecast System Reanalysis (CFSR) and China Meteorological Assimilation Driving Datasets (CMADS) have higher spatial resolution and are more easily accessible [24–26]. Additionally, both datasets are officially recommended weather data for the Soil and Water Assessment Tool (SWAT) hydrological model, ensuring their reliability. However, the accuracy of different precipitation products varies due to differences in data sources and interpolation algorithms in different regions [25,27]. Therefore, it is necessary to assess the applicability of CFSR and CMADS reanalysis meteorological products before conducting actual hydrological modeling.

The Jing River, the largest tributary of the Wei River, is located in the central part of the Loess Plateau, a semi-arid region in northwest China. The basin is influenced by the topography and geomorphology of the Loess hilly-gully region and the Loess highland-gully region, making it challenging to monitor hydro-meteorological data [28]. The basin faces severe soil erosion issues [29] and is frequently threatened by natural disasters such as landslides and debris flows [30,31]. Although the Chinese government has implemented large-scale afforestation and grassland restoration projects since 1999, leading to the recovery of vegetation cover and the control of soil erosion, the overall situation remains challenging [14,32,33]. Furthermore, under the influence of global climate warming, the ecological conditions and water resource characteristics in the basin have also undergone certain changes [34]. Therefore, accurately understanding the impact of climate and land-use change on hydrological processes is of great significance for maintaining the sustainable development and utilization of water resources.

Based on this premise, this study utilized the CFSR and CMADS datasets to drive the SWAT model, employing multiple scenario simulations to investigate the spatiotemporal dynamics of the impacts of climate and land-use changes on the characteristics of runoff in the Jing River Basin from 1999 to 2018. The objectives of this study were to: (i) evaluate annual average spatial distribution and intra-annual distribution of precipitation, maximum/minimum temperature among CFSR, CMADS, and OBS at various stations in the Jing River Basin utilizing spatial interpolation techniques; (ii) examine the suitability of CFSR, CMADS, and OBS datasets in hydrological simulations by employing the SWAT models aiming to achieve a more accurate depiction of the basin's meteorological conditions; and (iii) simulate the impact of land-use and climate change on runoff in the Jing River Basin through multiple scenario designs. The findings of this study can serve as a crucial foundation for water resources management and land-use planning in the context of climate change and human activities.

2. Materials and Methods

2.1. Study Area and Data

2.1.1. Study Area

The Jing River Basin is situated in the central region of the Loess Plateau within China, spanning coordinates 34°46′–37°19′ N and 106°20′–108°42′ E, encompassing an expansive basin area of 45,421 km^2. Geographically, it is characterized by the presence of

loess hills to the north, a loess plateau in the central region, mountainous terrain and dense forests to the southwest, and expansive river plains to the southeast (Figure 1). The basin experiences a typical temperate continental climate, with an average annual temperature of 8 °C and annual precipitation ranging from 400 to 600 mm. In terms of landforms, the basin predominantly consists of loess high plateau gully areas and hilly-gully areas, encompassing approximately 81% of the total area. These regions are significantly impacted by soil erosion, rendering them as primary sediment source areas for the Wei River. The Jing River Basin boasts an extensive water system, with its primary stream originating in Jing Yuan County, Ningxia Province. It traverses through Gansu Province before merging with the Wei River in Galling County, Shaanxi Province. Spanning a length of 483 km, the Jing River serves as a first-class tributary of the Wei River and a second-class tributary of the Yellow River. The control hydrographic station within the basin is Zhangjiashan Station, which oversees more than 95% of the basin's total area, covering a catchment area of 43,216 km^2.

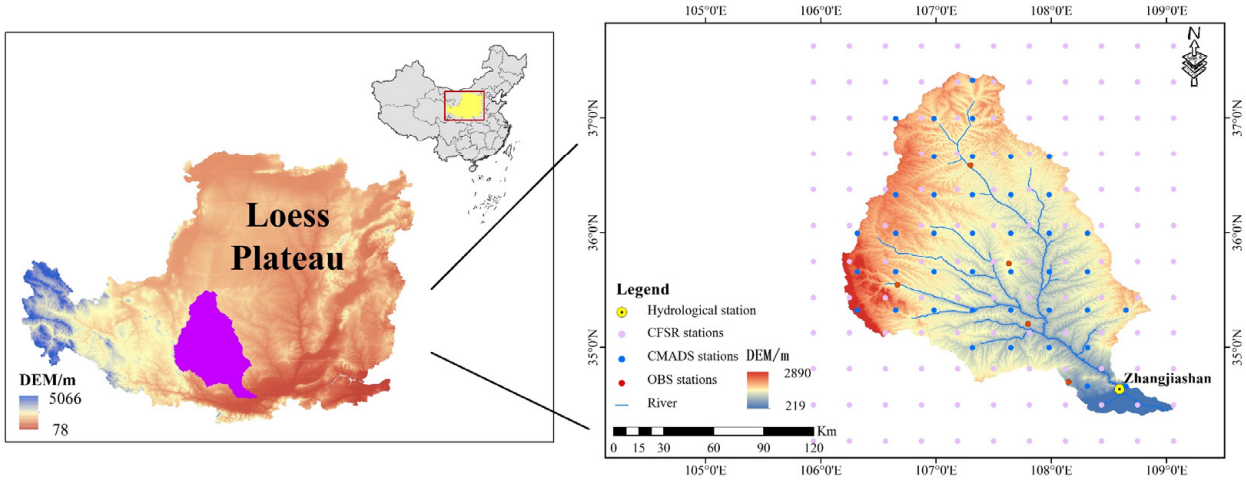

Figure 1. Location of Jing River Basin and distribution of meteorological and hydrological stations.

2.1.2. Data and Technical Framework

The following datasets were utilized for the present investigation:

(i) The digital elevation model (DEM) was acquired from the geospatial data cloud (http://www.gscloud.cn) with a spatial resolution of 30 m (accessed on 15 June 2022). The DEM of the Jing River Basin was obtained through preprocessing procedures such as projection conversion, cropping, and stitching in ArcGIS.

(ii) Soil data were obtained from the Chinese soil dataset V1.1 of the Harmonized World Soil Database (HWSD) (http://www.resdc.cn) with a spatial resolution of 1 km (accessed on 18 August 2022). The soil classification system employed primarily adhered to FAO-90 standards.

(iii) Land-use data were derived from Landsat TM/ETM remote sensing images as the primary source of information. These data were obtained from the Resource and Environment Science and Data Center of the Chinese Academy of Sciences (http://www.geodata.cn) and possessed a spatial resolution of 30 m (accessed on 11 October 2022).

(iv) The meteorological data incorporated the CFSR, CMADS, and OBS (Table 1). The CFSR and CMADS data, utilizing state-of-the-art data assimilation techniques to integrate traditional meteorological observatory and satellite radiation data, in conjunction with atmosphere–ocean–land–sea ice models, encompassed a wide array of data spanning multiple temporal scales.

Table 1. Information on three types of meteorological datasets that drive the SWAT model.

Data Type	CFSR	CMADS	OBS
Elements	(i). Daily maximum/minimum temperature; (ii). Daily accumulative precipitation; (iii). Daily accumulative solar radiation; (iv). Daily average wind speed; (v). Daily average relative humidity.		
Data spatial range of this study	34.19°~37.63° N, 105.94°~109.02° E	34.66°~37.33° N, 106.33°~108.66° E	34.46°~37.19° N, 106.20°~108.42° E
Data time range of this study	1 January 1999~31 December 2013 (daily)	1 January 1999~31 December 2018 (daily)	1 January 1999~31 December 2013 (daily)
Resolution ratio of this study	0.313°	0.333°	–
No. of stations applied by SWAT model	132	41	5
Download URL	https://swat.tamu.edu/data/cfsr (accessed on 15 March 2022)	http://www.cmads.org (accessed on 7 March 2022)	https://data.cma.cn (accessed on 12 January 2022)

(v) The hydrological observations from the Jing River Basin Hydrological Station were obtained from the Institute of Soil and Water Conservation, Northwest A&F University. This study collected monthly runoff observations from 1999 to 2018 at Zhangjiashan Station.

Based on the above datasets, the general structure of the technical framework for this study is illustrated in Figure 2.

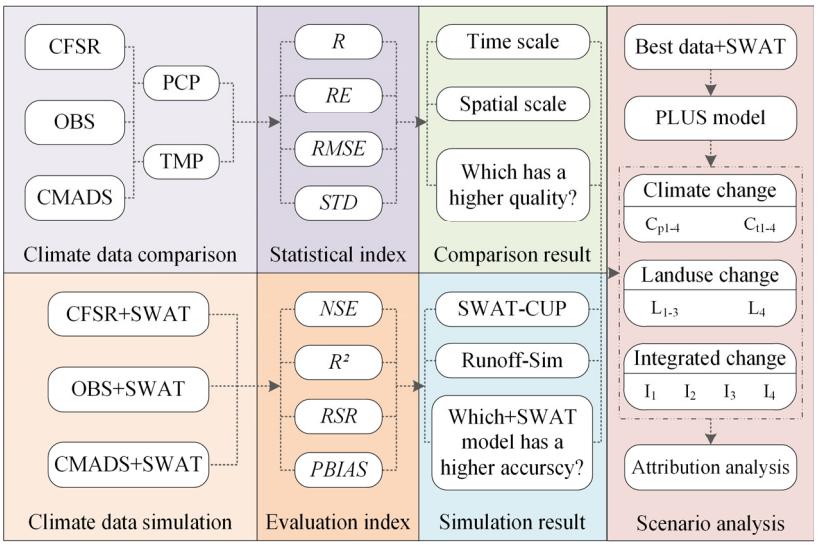

Figure 2. Technical framework employed in this study.

2.2. Spatial Interpolation Method

Spatial interpolation serves as a vital approach for acquiring meteorological element data across continuous spatial domains, utilizing known station data [35]. The ANUSPLIN interpolation software, grounded in the thin-slab spline interpolation theory, demonstrates exceptional capacity for accurately representing climate data surfaces. It is particularly well suited for the spatial interpolation of time-series meteorological data [36]. The theoretical formulation of the model is expressed as follows:

$$Z_i = f(x_i) + b^T y_i + e^i \quad (i = 1, 2, \cdots, N) \tag{1}$$

where Z_i is the dependent variable at a specific spatial location, such as precipitation or temperature; x_i is the vector of spline independent variables; f is the latent smooth function on x_i that requires estimation; y_i is the independent covariate; b^T is the coefficient; e^i is the

stochastic error associated with the independent variable; and N is the total number of observation points.

The reanalysis data for precipitation and maximum/minimum temperature were spatially interpolated to the exact station locations using the ANUSPLIN software. The reliability of the reanalysis data was initially assessed by utilizing statistical measures including the correlation coefficient (R), relative error (RE), root mean square error (RMSE), and standard deviation ratio (STD). For detailed assessment criteria, please refer to Section 2.4.2 "Model Calibration and Evaluation".

2.3. PLUS Model

The Patch-generating Land-use Simulation Model (PLUS) is an advanced model employed for simulating future land-use changes. This model combines the Land Expansion Strategy Analysis module (LEAS) with a multiclass stochastic patch-seed-based metacellular automata model known as CARS [37]. In this particular investigation (Figure 3), a comprehensive set of 16 raster drivers, including DEM, GDP, average annual temperature, average annual precipitation, and soil type, were utilized to characterize the alterations in the biological environment of the watershed. Subsequently, within the LEAS module, land-use expansion data were input, accompanied by the specification of various parameters (e.g., number of decision trees: 20, sampling rate: 0.02, number of training features: 16). The output from this module yielded the development probability for each land-use class. Furthermore, within the CARS module, specific parameters were input and meticulously adjusted. Notably, the attenuation threshold was set at 0.8, the diffusion coefficient was established as 0.3, and the probability of random seed was fixed at 0.0005. These settings facilitated the generation of a land-use map for the year 2030.

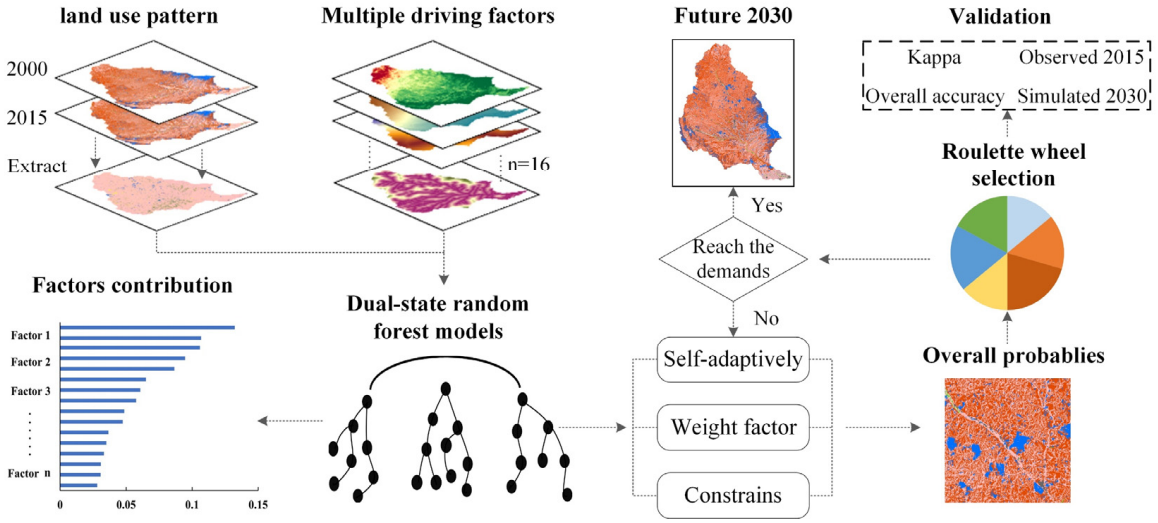

Figure 3. Land-use simulation framework based on the PLUS model.

2.4. SWAT Model

2.4.1. Model Setup

The spatial data projection was designated as WGS_1984_UTM_Zone_48N. During the extraction of the DEM river network, the inclusion of linear rivers from the second-transfer land-use database was employed to ensure the precision of the resulting river network. To derive an appropriate number of sub-basins and hydrological response units (HRUs), the minimum catchment area of rivers was established at 7500 ha through iterative refinement. Additionally, according to HWSD soil classification, soils were classified into 21 distinct groups (Figure 4a). Similarly, using the existing land-use classification, land-use was classified into 6 types (Figure 4b). Thresholds were imposed on land-use, soil type, and slope, with values set at 5%, 5%, and 10%, respectively. As a result, a total of 36 sub-

basins (Figure 4c) and 740 HRUs were generated. The meteorological elements required as inputs to the SWAT model, encompassing precipitation, maximum/minimum temperature, relative humidity, solar radiation, and wind speed, were all obtained at a daily scale. The selected time period to drive the SWAT model spanned from 1999 to 2013 (Table 1), which was consistent across all three datasets.

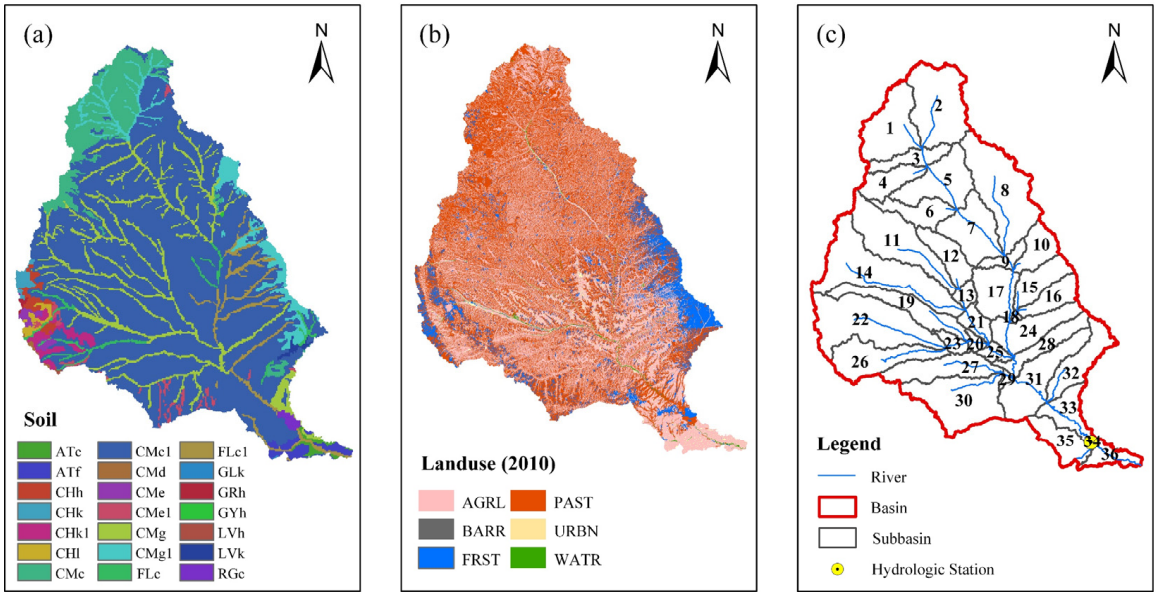

Figure 4. (**a**) Soil classification (ATc: cumulic anthrosols; ATf: fimic anthrosols; CHh: haplic chernozems; CHk, CHk1: calcic chernozems; CHl: luvic chernozems; CMc, CMc1: calcaric cambisols; CMd: dystric cambisols; CMe, CMe1: eutric cambisols; CMg, CMg1: gleyic cambisols; FLc, FLc1: calcaric fluvisols; GLk: calcic gleysols; GRh: haplic greyzems; GYh: haplic gypsisols; LVh: haplic luvisols; LVk: calcic luvisols; RGc: calcaric regosols), (**b**) land-use classification (AGRL: agriculture land; BARR: barren; FRST: forest; PAST: grassland; URBN: urban; WATR: water), (**c**) sub-basin delineation in the Jing River Basin.

2.4.2. Model Calibration and Evaluation

The SUFI-2 algorithm, incorporated within the SWAT-CUP software, was employed to optimize the parameters of the hydrological model driven by various modes [38]. A warm-up period from 1999 to 2000 was established to mitigate the influence of the initial simulation state. The calibration period spanned from 2001 to 2007, followed by a validation period from 2008 to 2013. Building upon the SWAT file and the prior sensitivity analysis, a total of 22 parameters associated with runoff were selected [11]. The final values of these model parameters were determined by iteratively simulating the model and adjusting the parameters after every 1000 iterations, based on recommended values and their initial limits (Table 2).

The determinacy coefficient (R^2), Nash–Sutcliffe efficiency coefficient (*NSE*), ratio of the root mean square error to the standard deviation of measured data (*RSR*), and percentage bias (*PBIAS*) were chosen as performance assessment metrics to evaluate the accuracy of runoff simulations [39] and gauge the suitability of the three datasets within the SWAT model (Table 3).

2.5. Setting Climate and Land-Use Change Scenarios

Based on the suitability assessment of reanalysis data, we chose the CMADS (1999–2018) dataset to drive the SWAT model due to its superior performance. After validating the model's simulation accuracy, we established three scenarios to analyze the response of Zhangjiashan Station runoff to watershed land-use and climate change (Table 4).

Table 2. Final values of different data-driven SWAT model parameters.

Parameter	Range	Final Value		
		CFSR+SWAT	**CMADS+SWAT**	**OBS+SWAT**
TRNSRCH.bsn	0–1	0.590	0.283	0.460
TIMP.bsn	0–1	0.855	0.598	0.782
SMFMX.bsn	0–20	10.005	7.814	17.493
SURLAG.bsn	0.05–24	16.876	12.463	15.552
SMFMN.bsn	0–20	11.940	18.300	19.084
GWQMN.gw	0–5000	2033.749	242.643	1127.715
GW_DELAY.gw	0–500	211.570	43.784	484.343
RCHRG_DP.gw	0–1	0.352	0.379	0.370
ALPHA_BF.gw	0–1	0.969	0.733	0.346
GW_REVAP.gw	0.02–0.2	0.036	0.148	0.105
LAT_TTIME.hru	0–180	7.313	28.178	30.277
EPCO.hru	0–1	0.777	0.815	1.000
SLSOIL.hru	0–150	1.435	3.649	0.148
OV_N.hru	0.01–30	37.824	6.814	4.892
ESCO.hru	0–1	0.206	0.175	0.063
CN2.mgt	35–98	93.783	77.171	81.117
CH_K2.rte	0.01–500	16.728	26.281	25.839
CH_N2.rte	0.01–0.3	0.024	0.065	0.029
ALPHA_BNK.rte	0–1	0.072	1.192	0.573
SOL_AWC().sol	0–1	0.577	0.666	0.662
SOL_K().sol	0–2000	735.605	741.229	902.798
TLAPS.sub	0–10	7.468	3.547	2.235

Table 3. Accuracy evaluation indicators in this study.

Index Name	Formula	Value Range	Optimal Value
Correlation Coefficient, *R*	$R = \frac{\sum_{i=1}^{n}(x_i-\overline{x})(y_i-\overline{y})}{\sqrt{\sum_{i=1}^{n}(x_i-\overline{x})^2\sum_{i=1}^{n}(y_i-\overline{y})^2}}$	[−1, 1]	1
Relative Error, *RE*	$RE = \frac{1}{n}\sum_{i=1}^{n}\frac{\lvert x_i-y_i\rvert}{y_i}$	[0, +∞]	0
Root Mean Square Error, *RMSE*	$RMSE = \sqrt{\frac{1}{n}\sum_{i=1}^{n}(x_i-y_i)^2}$	[-∞, +∞]	0
Standard deviation ratio, *STD*	$STD = \frac{\sqrt{\frac{1}{n}\sum_{i=1}^{1}(x_i-\overline{x})^2}}{\sqrt{\frac{1}{n}\sum_{n}^{1}(y_i-\overline{y})^2}}$	[0, 1]	1
Nash-Sutcliffe efficiency, *NSE*	$NSE = 1-\frac{\sum_{i=1}^{n}\left(Q_{o_i}-Q_{s_i}\right)^2}{\sum_{i=1}^{n}\left(Q_{o_i}-\overline{Q}_o\right)^2}$	[0, 1]	1
Coefficient of determination, R^2	$R^2 = \frac{\left[\sum_{i=1}^{n}\left(Q_{o_i}-\overline{Q}_o\right)\left(Q_{s_i}-\overline{Q}_s\right)\right]^2}{\sum_{i=1}^{n}\left(Q_{o_i}-\overline{Q}_o\right)^2\sum_{i=1}^{n}\left(Q_{s_i}-\overline{Q}_s\right)^2}$	[0, 1]	1

Table 3. *Cont.*

Index Name	Formula	Value Range	Optimal Value
Ratio of the root mean square error to the standard deviation of observed data, *RSR*	$RSR = 1 - \frac{\sqrt{\sum_{i=1}^{n}\left(Q_{o_i} - Q_{s_i}\right)^2}}{\sqrt{\sum_{i=1}^{n}\left(Q_{o_i} - \overline{Q}_o\right)^2}}$	[0, 1]	0
Percent bias, *PBIS*	$PBIAS = \frac{\left[\sum_{i=1}^{n}\left(Q_{o_i} - Q_{s_i}\right)\right]}{0.01 \times \sum_{i=1}^{n} Q_{o_i}}$	[0, 1]	0

Note: x_i and y_i denote the simulated and observed values at the actual meteorological site, respectively; $\overline{x}$ and $\overline{y}$ denote the mean simulated and mean observed values at the actual meteorological station, respectively; Q_{o_i} and Q_{s_i} denote the observed and simulated values of runoff, respectively; $\overline{Q}_o$ and $\overline{Q}_s$ denote the mean values of observed and simulated runoff, respectively; n is the number of statistical samples.

Table 4. Scenarios for modeling and analysis.

Climate change	Scenario	C_{00}	$C_{p/t1}$	$C_{p/t2}$	$C_{p/t3}$	$C_{p/t4}$
	Precipitation	0	−20%	−10%	+10%	+20%
	Temperature	0	−2 °C	−1 °C	+1 °C	+2 °C
Land-use change (km^2)	Scenario	L_0	L_1	L_2	L_3	L_4
	AGRL	20,164.2	44,438.4	—	—	17,800.3
	FRST	4160.9	—	44,438.4	—	5189.2
	PAST	20,111.8	—	—	44,438.4	20,925.4
	WATR	203.5	203.5	203.5	203.5	181.4
	URBN	779.1	779.1	779.1	779.1	1297.4
	BARR	1.5	—	—	—	27.2
Integrated change	Scenario	Land-use data			Meteorological data	
	I_1	2000			1999–2010	
	I_2	2015			2011–2018	
	I_3	2000			2011–2018	
	I_4	2015			1999–2010	

(i) Climate change scenarios: Based on the IPCC Sixth Assessment Report and the potential range of future climate changes in the watershed [40,41], we established benchmark intervals of 10% for precipitation and 1 °C for temperature. This formed the basis for configuring eight climate change scenarios: precipitation scenarios C_{p1}–C_{p4} and temperature scenarios C_{t1}–C_{t4}, aimed at analyzing the impact of climate change on runoff.

(ii) Land-use change scenarios: Using the land-use status from the year 2000 [14] as a baseline, we employed the PLUS model to forecast the watershed's land-use changes under a natural development scenario for 2030 (L_4). Additionally, we established extreme scenarios (L_1–L_3) pertaining to specific land-use types to delve deeper into the influence of individual land-use changes on runoff volume, while mitigating the impact of other variables.

(iii) Integrated change scenarios: The climate change process in the Jing River Basin has been relatively gradual, and watershed conservation measures like afforestation and farmland conversion were not in place before the 21st century. Thus, scenarios were designated for the periods 1999–2010 and 2011–2018 (I_1–I_4). Using I_1 as the reference period, the comparison of I_3 with I_1 can be employed to analyze the influence of climate change on runoff. Similarly, the comparison of I_4 with I_1 can be utilized to assess the impact of land-use change on runoff. Furthermore, the analysis of the impact of both changes on runoff can be conducted by comparing I_2 with I_1.

3. Results

3.1. Comparison and Evaluation of CMADS and CFSR Data

3.1.1. Spatial Distribution of Multi-Year Average Precipitation and Temperature

Utilizing the ANUSPLIN interpolation software, we obtained the spatial distribution of the reanalysis data for the Jing River Basin encompassing the multi-year average precipitation and maximum/minimum temperature from CMADS, CFSR, and OBS sources, spanning the period of 1999–2013 (Figure 5). The lower part of the basin, particularly the southeastern region encompassing Liquan County, experienced elevated temperatures and abundant precipitation owing to the influence of a temperate continental monsoon climate. Regarding precipitation, the CMADS dataset exhibited an underestimation in total annual average precipitation, whereas the CFSR dataset tended to overestimate it in comparison to OBS. Concerning the area of maximum precipitation, CMADS closely aligns with OBS, while CFSR exhibited a slight northwest displacement. Nonetheless, when precipitation was not considered, both CMADS and CFSR exhibited spatial distributions similar to OBS, characterized by a decreasing trend from southeast to northwest. This implied higher precipitation in the mountainous and river plain areas to the south, and lower precipitation in the loess plateau and hilly regions to the north.

Regarding maximum/minimum temperature, all three meteorological datasets exhibited a gradual rise from the north to the south, spanning from the loess hilly regions to the river plain areas. This indicated that the spatial distribution of temperature was primarily influenced by factors such as latitude and altitude. Maximum temperatures ranged from 26 °C to 42 °C, while minimum temperatures ranged from −25 °C to −7 °C. When considering both the values and distribution areas of maximum/minimum temperature, CMADS demonstrated a closer resemblance to OBS than CFSR, albeit with a slight northwestward displacement of maximum/minimum temperatures. In conclusion, CMADS outperformed CFSR in terms of accuracy and spatial distribution representation for multi-year average precipitation and temperature.

3.1.2. Intra-Annual Distribution of Precipitation and Temperature

The observed variation pattern of average intra-annual distribution for precipitation and maximum/minimum temperature are evident in Figure 6. It demonstrated a distinct cycle of increasing and then decreasing trends, specifically indicating higher precipitation and temperatures during summer and autumn (June to November), and lower precipitation and temperatures during spring and winter (December to May). Furthermore, it is noteworthy that CMADS consistently exhibited lower levels of precipitation and maximum/minimum temperature compared to OBS across all months. Conversely, CFSR generally displayed higher maximum/minimum temperatures than OBS throughout the year, with CFSR consistently overestimating when the average monthly precipitation was below 80 mm. This aligns with the spatial distribution depicted in Figure 5, and the underlying reasons will be examined in the forthcoming discussion section.

Upon examining the statistical indicators derived from the five stations within the basin, it became apparent that both reanalysis data sources exhibited a high correlation with the observed data, exceeding an R of 0.97. Evaluating the RE and RSE, the disparity between CMADS and CFSR in terms of the maximum temperature impact was not significant. However, for precipitation and minimum temperature, CMADS displayed smaller values that were in closer proximity to OBS. Analyzing the STD, it was evident that CMADS achieved superior values of 0.98, 1.03, and 0.97 for precipitation, maximum temperature, and minimum temperature, respectively. In contrast, CFSR yielded values of 0.84, 1.11, and 1.19, respectively, further deviating from the optimal value of 1. Consequently, despite CMADS exhibiting slight underestimation in monthly average precipitation and maximum/minimum temperature compared to OBS, the statistical outcomes of each indicator ascertained that CMADS demonstrated greater concurrence with OBS when compared to CFSR.

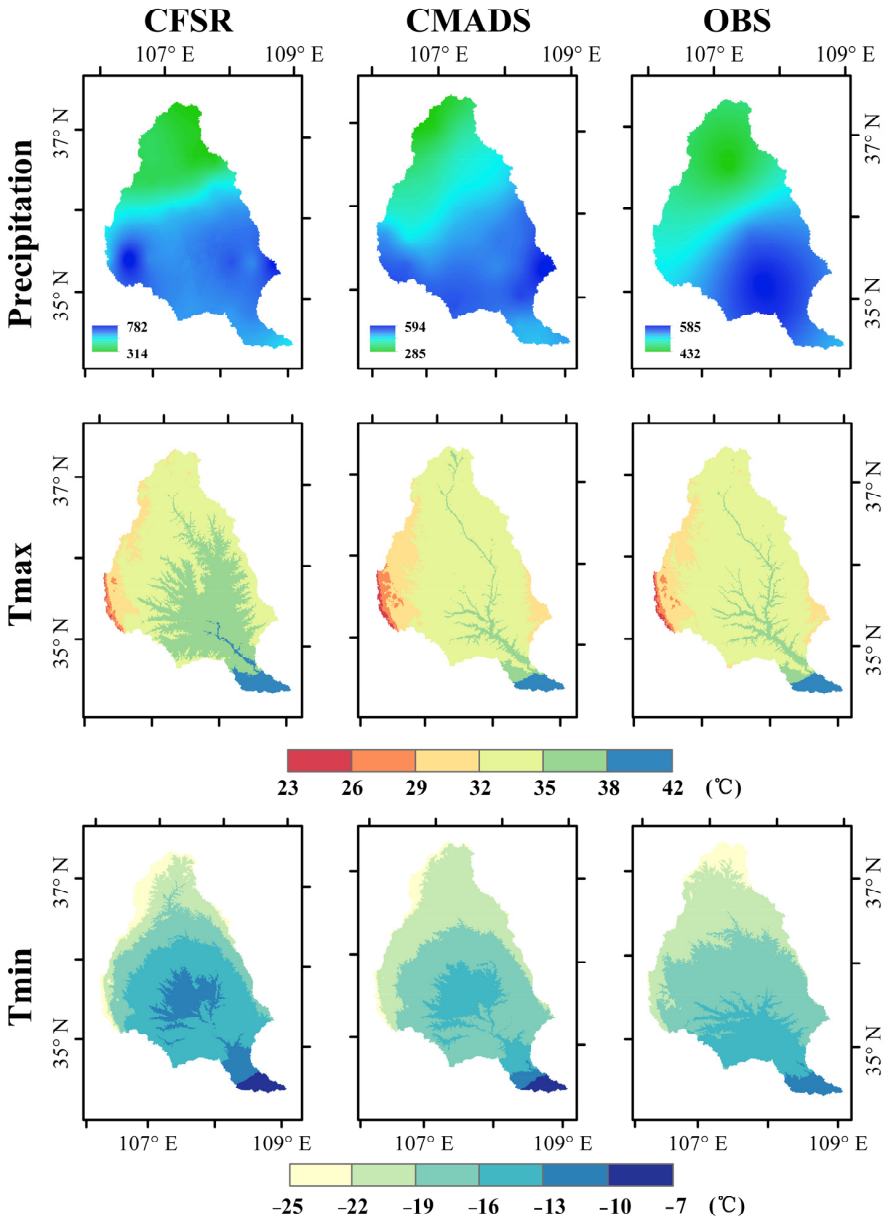

Figure 5. Spatial distribution of CMADS, CFSR, and OBS in Jing River Basin: the first, second, and third rows of the figure represent the spatial distribution of annual average precipitation, maximum temperature, and minimum temperature, respectively.

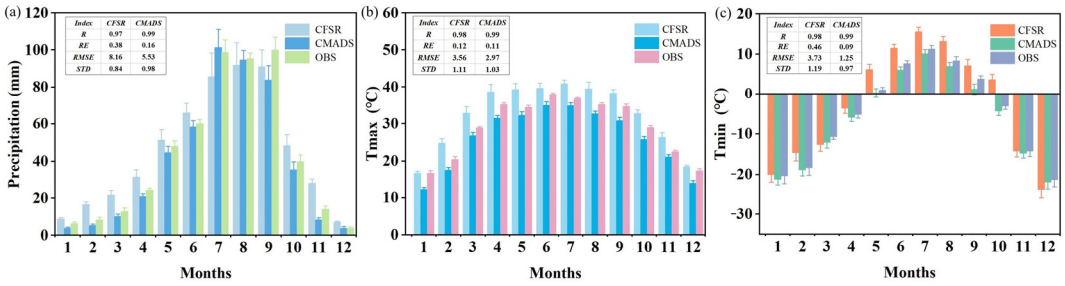

Figure 6. Intra-annual distribution of 3 types of meteorological data in the Jing River Basin (error bars indicate standard errors): (**a**) intra-annual distribution for precipitation, (**b**) intra-annual distribution for maximum temperature, (**c**) intra-annual distribution for minimum temperature.

3.2. Effects of Runoff Simulation in SWAT Models Driven by Different Datasets

The aforementioned three datasets served as input for the hydrological model, and the SWAT model was independently employed to generate monthly simulation results of runoff for the Zhangjiashan hydrological station (Figure 7). The *NSE* values for the CFSR, CMADS, and OBS+SWAT models during the rate regular/validation periods were 0.66/0.70, 0.82/0.84, and 0.80/0.79, respectively. Similarly, the R^2 values were 0.66/0.74, 0.84/0.85, and 0.81/0.78; the *RSR* values were 0.53/0.50, 0.42/0.41, and 0.43/0.46; the *PBIAS* values were 11.2/9.7, 2.6/0.9, and 5.9/3.2, in the same order. These results were evaluated according to the criteria established by Moriasi et al. [39]. It can be concluded that the CMADS and OBS+SWAT models exhibited excellent performance for both the calibration period and validation period at the Zhangjiashan Station when compared to the CFSR model. However, the CFSR+SWAT model demonstrated relatively poor simulation during the calibration period, while achieving a relatively better performance during the validation period.

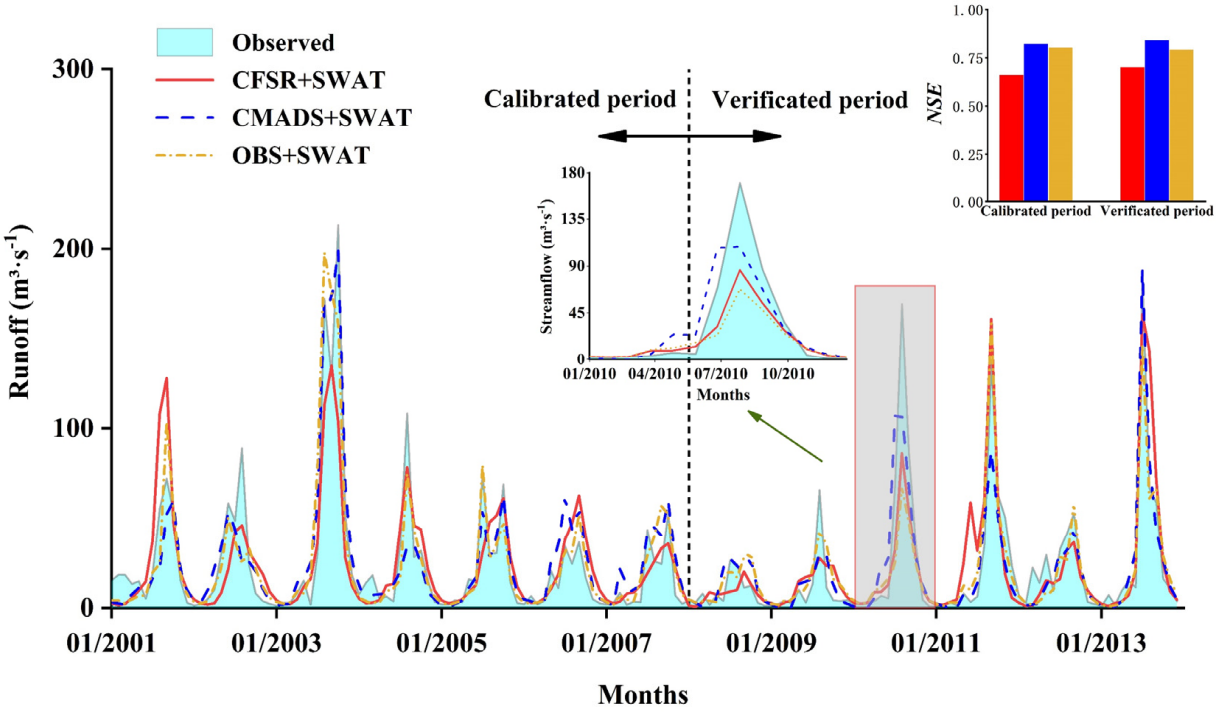

Figure 7. Comparison of monthly runoff simulation results from different meteorological data-driven SWAT models.

The peak runoff values predominantly occurred during the months of July to September, aligning with the intra-annual precipitation distribution in the basin. This pattern was particularly evident in the simulation results for the peak runoff in 2001 and 2003. A comparison between CFSR and OBS data on the multi-station monthly average precipitation in July to September within the basin revealed that the CFSR data overestimated the observed precipitation by approximately 11.3 mm (+10.9%) in 2001 while underestimating it by about 79.8 mm (−32.7%) in 2003. It was discovered that the underestimated precipitation in 2003 coincided with a rare meteorological event known as the "West China Autumn Rain," which affected the middle and lower reaches of the Yellow River from late August to mid-October, resulting in several flood peaks in the Jing River Basin, including the highest recorded flood level at the Zhangjiashan hydrological station. Furthermore, the year 2010 experienced abundant precipitation during July to September, leading to a significant flood event. Conversely, the intensity of precipitation was relatively weaker in 2003, where the CFSR data underestimated the observed precipitation by approximately 41.3 mm (−19.3%) during that month.

Due to the conspicuous occurrence of overestimation of low precipitation and underestimation of high precipitation by the CFSR dataset, the multi-year average precipitation for July–September was lower than the observed precipitation (Figure 6). Consequently, the simulated baseflow tended to be overestimated, while the peak runoff was typically underestimated. This phenomenon was particularly pronounced in the time span between 2005 and 2010, resulting in poor runoff simulation outcomes for the CFSR+SWAT model. Conversely, the runoff simulation results for the CMADS+SWAT and OBS+SWAT models exhibited higher quality and demonstrated similarities during the same period. In conclusion, the CMADS+SWAT model proved to be more adept at fitting the observed runoff and enhancing the precision of runoff simulations.

3.3. Impacts of Climate and Land-Use Change on Runoff

3.3.1. Climate Change Scenarios

The meteorological data obtained from CMADS covering the period of 1999–2018, along with the land-use data from 2000, were employed as the foundational period to derive simulation results for various climate change scenarios (Figure 8a,b). The interannual patterns of runoff under different climate scenarios exhibited consistency, with the highest runoff occurring in 2003 (C_{p4} = 104.1 m^3/s) and the lowest in 2009 (C_{p1} = 8.5 m^3/s). When comparing temperature and precipitation scenarios, the differences in runoff were more pronounced under the precipitation scenario. The overall simulation results revealed distinct interannual variations and followed a specific pattern: $C_{p4} > C_{p3} > C_{p0} > C_{p2} > C_{P1}$ (Figure 8a), $C_{t1} > C_{t2} > C_{00} > C_{t3} > C_{t4}$ (Figure 8b). Maintaining a constant temperature, a 10% and 20% increase in precipitation led to a corresponding average annual runoff increase of 23.22% and 50.62%, respectively. On average, for every 10% increase in precipitation, runoff increased by 25.31%. Conversely, a decrease in precipitation resulted in a decrease in average annual runoff (Table 5). These findings demonstrated a direct proportional relationship between average annual runoff and changes in precipitation, emphasizing the direct impact of precipitation on basin flow production. Keeping precipitation constant, a decrease of 1 °C and 2 °C in temperature led to an average annual runoff increase of 2.27% and 4.83%, respectively. Conversely, an increase in temperature resulted in a decrease in average annual runoff. On average, for every 1 °C increase in temperature, runoff decreased by 0.64%. This revealed an inverse proportional relationship between average annual runoff and changes in temperature, highlighting the indirect influence of temperature on runoff through increased evaporation.

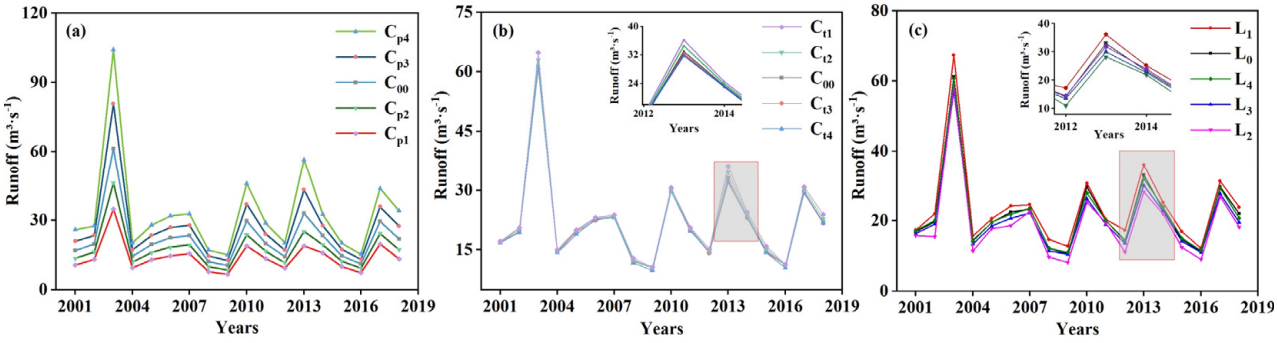

Figure 8. Annual runoff at Zhangjiazhan Station under different change scenarios: (**a**) precipitation change scenarios: C_{p0} to C_{p4}, (**b**) temperature change scenarios: C_{t0} to C_{t4}; (**c**) land-use change scenarios: L_0 to L_4.

Table 5. Simulation results of runoff under different scenarios (m^3/s).

Type	Scenario	Mean Annual Runoff	Runoff Change Rate
Precipitation change	C_{p4}	33.29	50.62%
	C_{p3}	27.24	23.22%
	C_{00}	22.10	—
	C_{p2}	17.77	−19.59%
	C_{p1}	14.03	−36.50%
Temperature change	C_{t4}	21.82	−1.27%
	C_{t3}	22.03	−0.34%
	C_{00}	22.10	—
	C_{t2}	22.60	2.27%
	C_{t1}	23.17	4.83%
Land-use change	L_0	22.10	—
	L_1	24.04	8.78%
	L_2	19.46	−11.95%
	L_3	20.71	−6.29%
	L_4	21.92	−0.81%

Type	Scenario	Mean annual		Effects of		Effects of
		Precipitation	Temperature	Runoff	Land-use	climate
Integrated change	I_1	488.51 mm	9.76 °C	22.89	—	—
	I_2	447.68 mm	10.08 °C	21.65	−0.12	−1.12
	I_3	—	—	21.77	—	−1.12
	I_4	—	—	22.77	−0.12	—

3.3.2. Land-Use Change Scenarios

Comparing the actual 2015 land-use data of the Jing River Basin with simulated land-use data from the PLUS model yielded a Kappa value of 0.935 and an overall accuracy of 0.966, indicating a high level of confidence in the simulation results [37]. Thus, using the 2015 actual land-use as a foundation, the PLUS model was employed to simulate the 2030 land-use pattern under the scenario of natural development in the Jing River Basin (Figure 9a). Additionally, a Sankey diagram was constructed (Figure 9b) using the land-use transfer matrix spanning from 2000 to 2030 to visually depict the transitions between different land-use types during various time intervals. The findings indicated that, between 2005 and 2015, there was a heightened frequency of conversions between land-use categories. During this period, arable land experienced a substantial reduction, with 66.3% of the area transitioning to grassland, 19.8% to construction land, and 13.4% to forest land. Notably, the watershed area decreased by 11.8 km^2, primarily attributable to a 3.6 km^2 transfer out of arable land. Conversely, the area of forest land, grassland, and construction land witnessed an increase, with construction land experiencing the most significant growth at 35.8%. This expansion is likely linked to the rapid socioeconomic development and urban transformation. From 2015 to 2030, various degrees of area transfers occurred among the categories. Arable land continued to decline by 1076.8 km^2, while other land categories exhibited varying degrees of expansion. Forest land experienced the most substantial increase, spanning 1028.3 km^2, followed by construction land with a growth of 66.5%. During both time periods, there were transfers of land from other categories to construction land, amounting to 474.1, 8.6, 30.1, 5.5, and 0.1 km^2, respectively. Moreover, water areas underwent conversions to other land types, with respective areas of 7.1, 3.9, 4.1, 5.5, and 1.4 km^2.

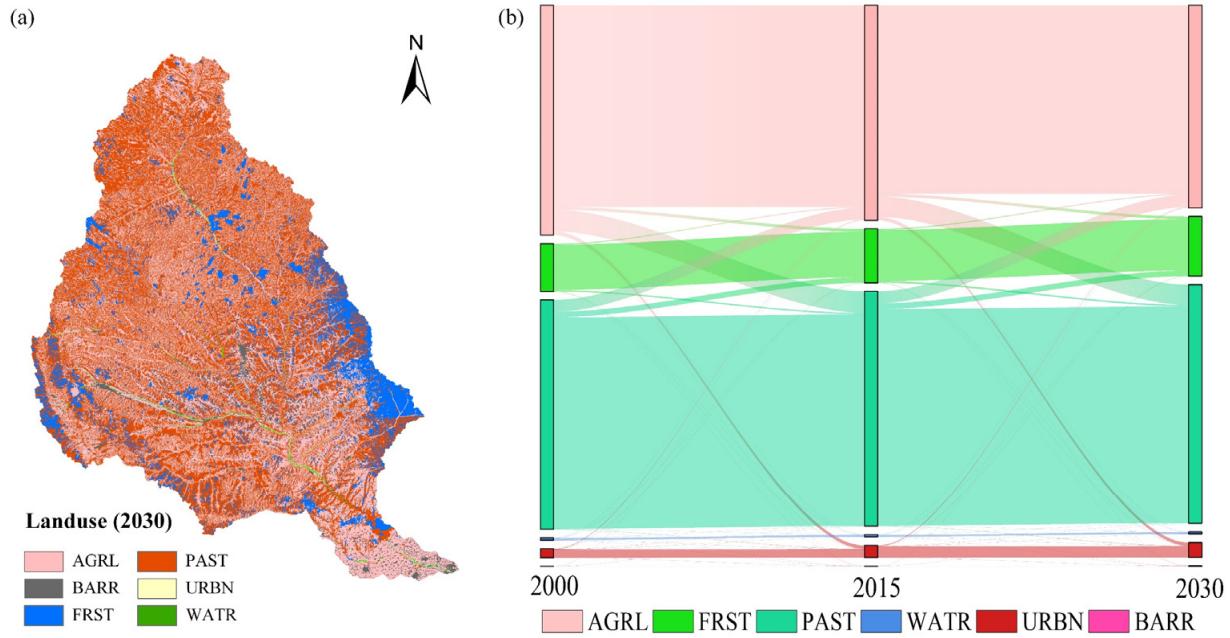

Figure 9. Schematic diagram of land-use type in Jing River Basin: (**a**) land-use in 2030, (**b**) land-use type transformation in 2010–2030.

Notably, the interannual runoff trends under different land-use scenarios exhibited a consistent pattern. The highest runoff value occurred in 2003, denoted as L_1 = 67.32 m^3/s, while the lowest runoff value was observed in 2009, denoted as L_2 = 8.17 m^3/s. In comparison to diverse climate scenarios, the variation in runoff under different land-use conditions demonstrated a moderate level. The overall pattern of interannual variation in the simulation results followed the sequence: $L_1 > L_0 > L_4 > L_3 > L_2$ (Figure 8c). The outcomes of the extreme land-use type scenario indicated an 8.78% increase in runoff for L_1, while L_2 and L_3 experienced decreases of 11.95% and 6.29%, respectively. It was evident that farmland exerted a flow-increasing effect, whereas grassland and woodland had an intercepting effect on watershed runoff, with woodland exhibiting a stronger interception intensity. This highlighted the significant influence of vegetation cover on hydrology. Regarding L_4, the simulation results projected a decrease in Zhangjiashan's runoff volume from 22.10 m^3/s to 21.92 m^3/s by 2030 under natural development, reflecting a decline of 0.81%. This reduction was attributed to the decrease in arable land area and the increase in forest and grassland areas in 2030.

3.3.3. Integrated Climate and Land-Use Change Scenarios

The monthly runoff simulation results under the integrated climate and land-use change scenario are depicted in Figure 10. It was evident from the results that the simulated peak flood season at Zhangjiashan hydrological station deviated from the observed values in certain years. Specifically, the simulated values were lower than the observed values in 2003, 2004, 2010, and 2018, while they were higher than the observed values in 2006, 2008, 2014, and 2017. The simulation accuracy was deemed satisfactory as indicated by $R^2 > 0.8$, $NSE > 0.76$, $RSR < 0.45$, and $PBIAS < 10\%$, meeting the criteria for good performance established by Moriasi et al. [39]. These findings demonstrated the favorable applicability of the CMADS+SWAT model in the Jing River Basin.

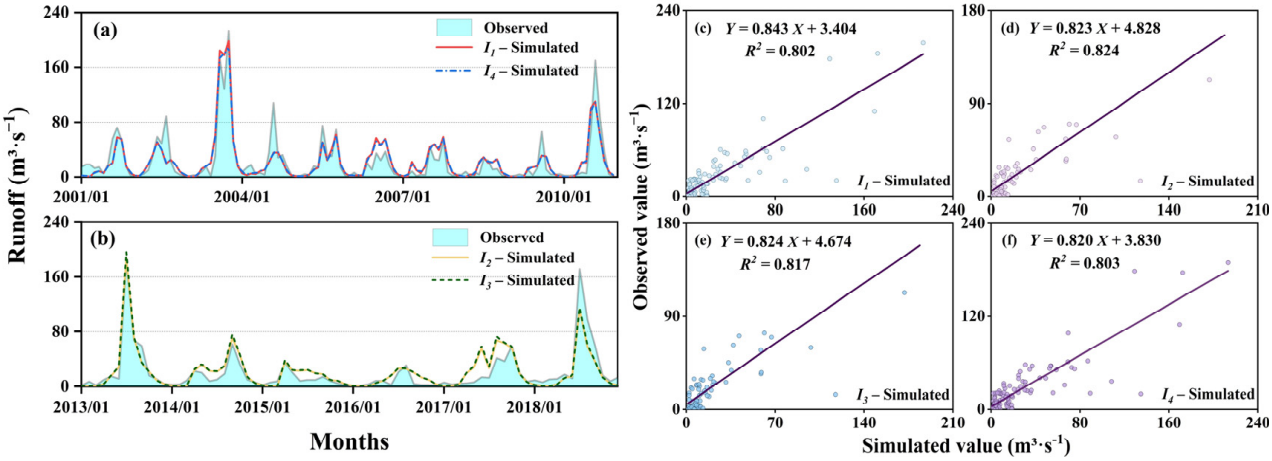

Figure 10. Comparison of simulated and observed monthly runoff at Zhangjiashan Station under the integrated scenario: (**a**) Runoff simulation effects for scenarios I_1 and I_4, (**b**) Runoff simulation effects for scenarios I_1 and I_4, (**c**) Correlations for scenario I_1, (**d**) Correlations for scenario I_2, (**e**) Correlations for scenario I_3, (**f**) Correlations for scenario I_4.

The results of the integrated scenario analysis (Table 5) reveal the average annual runoff values for scenarios I_1, I_2, I_3, and I_4 to be 22.89 m^3/s, 21.65 m^3/s, 21.77 m^3/s, and 22.77 m^3/s, respectively. Comparing scenario I_2 with I_1, it was evident that the combined influence of land-use and climate change led to a decrease in the average annual runoff by 1.24 m^3/s. In scenario I_3, the average annual temperature rose by 0.32 °C (+3.3%), while the average annual precipitation experienced a decrease of 40.83 mm (−8.4%), with a more pronounced reduction observed. Scenario I_4, when compared to scenario I_1, demonstrated a decrease in the area of cultivated land, an increase in the area of construction land, and an increase in the area of grassland and forest land. Comparing scenarios I_3 and I_4 with scenario I_1, it became apparent that climate change contributed to a reduction of 1.12 m^3/s in the annual average runoff, while land-use change accounted for a decrease of 0.12 m^3/s in the annual average runoff.

4. Discussion

4.1. Comparison and Evaluation of CMADS and CFSR Data in Runoff Modeling

The inclusion of meteorological data as input is of paramount importance in hydrological model simulations, as errors in such data can significantly impact the accuracy of hydrological output [42]. Both CMADS and CFSR exhibited temperature values that closely aligned with observations, with CMADS demonstrating particularly favorable performance, as indicated by average *RMSE* values ranging from 1.25 °C to 2.97 °C. In terms of precipitation, the average *RMSE* values for CMADS and CFSR were 5.53 and 8.16 mm, respectively, showcasing higher uncertainties. The annual average spatial distribution of precipitation and maximum/minimum temperature exhibited similarity across all three meteorological datasets (Figure 5). However, in terms of the annual average temperature and total precipitation, CMADS displayed slight underestimation, while CFSR showed slight overestimation. These observations aligned with the average intra-annual distribution outcomes (Figure 6). The underestimation of precipitation in CMADS stemmed from the utilization of the CMORPH satellite precipitation product as the background field, which led to the neglect of precipitation below 4 mm due to surface reflectivity constraints [43,44]. Conversely, the overestimation of precipitation in CFSR could be attributed to the absence of correction for observations obtained from meteorological stations within the study area. The interplay of topography, climate prognostic models, and systematic errors contributed to the overestimation of day-by-day rainfall and an increased number of rainfall days in CFSR [22]. Additionally, all three meteorological datasets exhibited

substantial precipitation fluctuations, with a pronounced uneven distribution throughout the year. Notably, summer and autumn witnessed the highest precipitation levels, accounting for approximately 70% to 80% of the total, while spring experienced relatively lower precipitation, accounting for approximately 20%, and winter received almost no precipitation. This pattern was primarily attributable to the location of the Jing River Basin, which lay on the periphery of the summer monsoon zone and was highly susceptible to the interaction between the Iranian high pressure, western Pacific subtropical high pressure, and the cold trough beneath the southeast of Siberia [45].

Reanalysis meteorological products derived from CFSR and CMADS were valuable sources of data for hydrological analysis, particularly for watersheds lacking direct measurements. Consequently, there was a growing interest in assessing the accuracy and applicability of these data. Previous studies had evaluated meteorological products through comparisons with rainfall gauges, rainfall records, and their performance in hydrological modeling [23,46,47]. In our study, we employed the AUSPLIN interpolation method to compare the spatial distribution of the two reanalyzed precipitation products and validated their suitability at the point level using measurements from five meteorological stations. However, due to the absence of observed meteorological data in the eastern part of the basin, directly evaluating the quality of precipitation products for the entire basin remained challenging. To address this, we employed the SWAT hydrological model approach while maintaining constant settings. By comparing the differences in hydrological simulations, specifically the performance of the runoff process observed at Zhangjiashan Station, we were able to infer the quality of the precipitation data products. Our findings indicated significant disparities in the runoff simulations driven by CFSR, CMADS, and OBS+SWAT. CMADS exhibited the highest performance, with *NSE* reaching as high as 0.82/0.84 for the calibration/validation periods. On the other hand, CFSR performed less favorably, with *NSE* values of only 0.66/0.73. Based on the evaluation criteria developed by Moriasi et al. [39], the CMADS, OBS+SWAT model yielded very good results during both the calibration and validation periods at Zhangjiashan Station, while the CFSR+SWAT model produced good results. This led us to conclude that the carefully calibrated SWAT model was well suited for the Loess Plateau region in northwest China [14,48]. Analysis of monthly runoff simulation maps revealed that the maximum runoff values generated by the three models typically occurred between July and September, aligning with the intra-annual distribution of precipitation in the watershed. With CMADS, the runoff simulations were more accurate during years with higher rainfall, while slight underestimation was observed during years with lower rainfall (Figure 7). This discrepancy could be attributed to the fact that the monthly average precipitation of CMADS during the study period was significantly lower than the monthly average rainfall of OBS and CFSR. As for CFSR, its tendency to overestimate low precipitation and underestimate high precipitation led to overestimated baseflow and underestimated peak runoff, resulting in suboptimal simulation outcomes. These findings aligned with previous studies, such as the research conducted by Tan et al. [25], which indicated that CFSR precipitation tended to overestimate SWAT simulated flows in Asian, African, and mountainous basins [25]. Additionally, Ning discovered that CMADS underestimated precipitation in the southern basin of East China [43], while Wang found runoff underestimation in the CMADS-driven SWAT model for the West River basin, particularly concerning peak flood flow [23].

The outcomes of the comprehensive comparison and evaluation of CMADS and CFSR data for runoff simulations revealed that CMADS exhibited superior accuracy in multi-year average precipitation and temperature compared to CFSR. Additionally, CMADS demonstrated a more precise depiction of spatial distribution, establishing it as a dependable dataset in the absence of observed data. Moreover, the calibrated SWAT model proved to be well suited for the Loess Plateau region in China, and the CMADS+SWAT model enhanced the fitting of observed runoff, thereby improving the accuracy of runoff simulation.

4.2. Assessing Impacts of Climate and Land-Use Changes on Runoff Simulation

To conduct a more detailed analysis of whether the effects of climate and land-use changes on runoff varied across sub-basins, we examined the average annual water yield at the sub-basin level using the natural break point grading method (Figure 11). Regions with high average annual water yield were primarily situated in the western valley and southeastern mountainous area, particularly in sub-basins 10, 26, 30, and 32. Conversely, areas with lower water yield were mainly found in the loess hills and ravines in the upper reaches of the Malian River in the northwest, predominantly in sub-basins 1 and 2. Overall, the spatial distribution pattern closely mirrored that of precipitation (Figure 5), with higher precipitation corresponding to higher water yield. This indicated that precipitation served as the primary source of runoff in the Jing River. The average annual water yield under scenarios of precipitation/temperature change, land-use change, and integrated change ranged from 38 to 210/54 to 166, 41 to 147, and 55 to 144 mm, respectively. These findings suggest that the range of water yield change resulting from climate change was greater than that caused by land-use change. Specifically, in the scenario simulation of climate change, water yield increased with rising precipitation and decreased with increasing temperature. This correlation was significant and aligned with the runoff trend (Figure 8). The response of runoff to changes in precipitation was more sensitive than to changes in temperature. This was attributed to the fact that runoff in the watershed, situated within the temperate continental climate of the Loess Plateau, was predominantly replenished by precipitation, which directly impacted runoff. Temperature, on the other hand, exerted an indirect influence on runoff [49]. Regarding simulated land-use change scenarios, the average annual water yield for the L_1, L_2, L_3, and L_4 scenarios ranged from 56 to 147, 41 to 122, 44 to 127, and 55 to 138 mm, respectively, with the maximum value occurring in sub-basin 32 concurrently. Compared to the base period's water yield (54 to 140 mm), L1 generally exhibited an increase, while L_2 and L_3 generally showed a decrease. The change pattern was similar (Figure 8), indicating that vegetation cover influenced the hydrological process, with cultivated land contributing to increased flow, while grassland and woodland intercepted runoff within the watershed. Woodland exhibited a stronger interception capacity. In the integrated change scenario simulation, the water yield of I_1 and I_4, and of I_2 and I_3 displayed similar patterns at the sub-basin level, respectively. The distribution and changes in water yield under integrated change resembled those under climate change alone. Compared to I_1, the average annual runoff of I_2 decreased by a total of 1.24 m^3/s, with climate change accounting for 90.3% and land-use change accounting for 9.7% of the reduction. This indicates that changes in water production and runoff were primarily driven by climate change and were less influenced by land-use, consistent with previous research [50]. However, the impact of land-use on runoff should not be disregarded. The increase in woodland and grassland area had a mitigating effect on runoff, as both woodland and grassland possessed the ability to intercept and retain water [13,34]. Notably, a large-scale project focused on converting farmland back to forest and grass was implemented in the Loess Plateau region since 1999 [14].

The findings regarding the integrated impact of climate and land-use changes on runoff revealed the necessity of implementing proactive flood control measures in the Loess Plateau region of the basin. This includes implementing real-time monitoring and early warning systems for heavy precipitation in sub-basins 10, 26, 30, and 32, as well as adopting suitable precautionary measures in the future. Furthermore, special attention should be given to the encroachment of cultivated land on forest and grassland areas. Implementing measures such as the conversion of cultivated land back to forest and grassland is a crucial strategy for effective flood control. Additionally, it is imperative to undertake rational land-use planning and optimize the layout of land utilization to mitigate the hydrological consequences, particularly the adverse impacts, resulting from climate change within the basin.

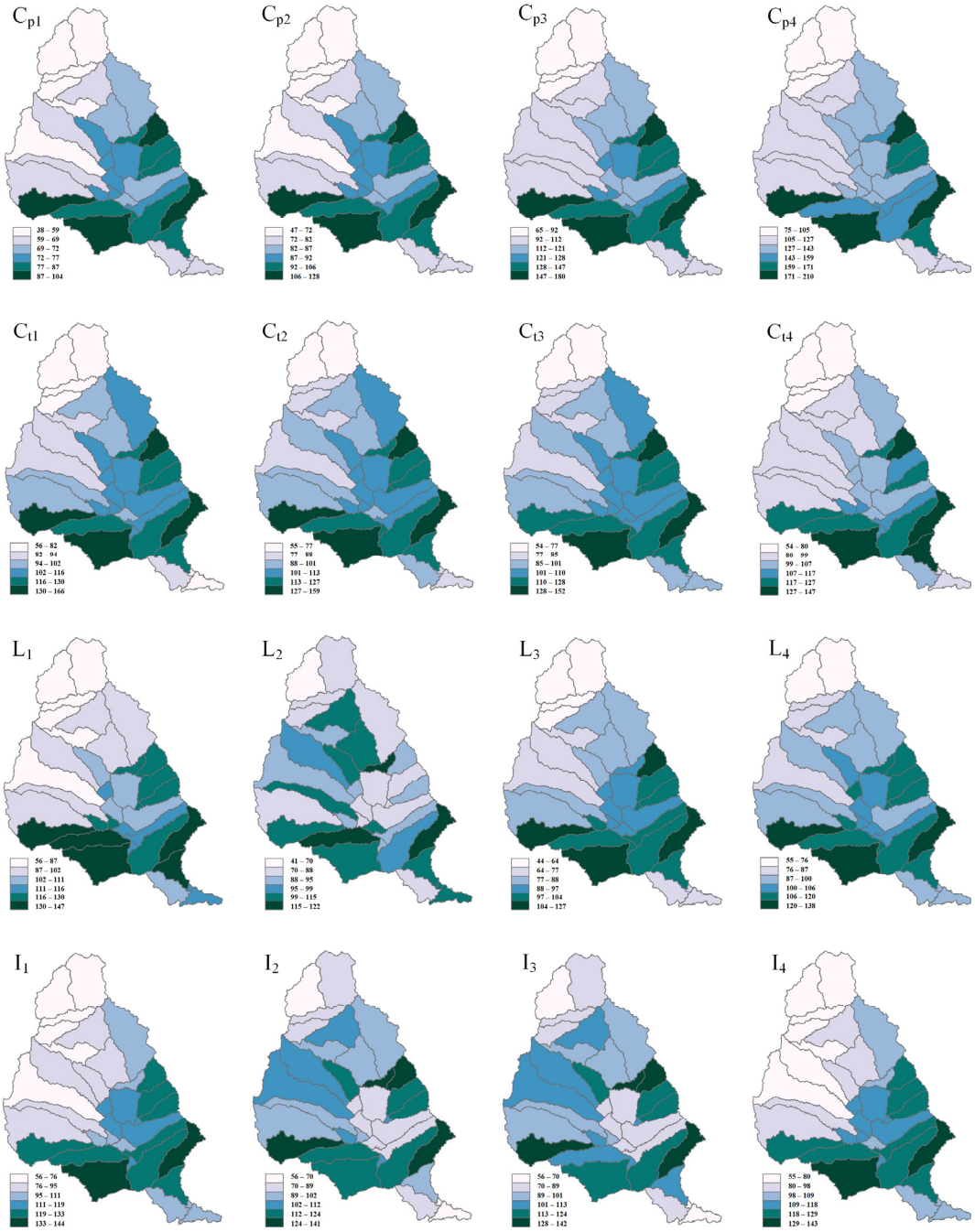

Figure 11. Analysis of water production under different scenario models (mm): the **first row** indicates **C_{p1}–C_{p4}** for different precipitation scenarios, 38–210 mm; the **second row** indicates **C_{t1}–C_{t4}** for different temperature scenarios, 56–147 mm; the **third row** indicates **L_1–L_4** for different land-use scenarios, 56–138 mm; and the **fourth row** indicates **I_1–I_4** for integrated scenarios, 56–143 mm.

4.3. Limitations of This Study

This study possesses certain limitations, encompassing the following two aspects:

(i) CMADS and CFSR reanalysis data were chosen as the input data for the hydrological model, but their uncertainty exerted a significant influence on the results of the runoff simulation [51,52]. Additionally, the land cover and soil parameters in the SWAT model adhere to the USGS standards, which differ considerably from the Chinese classification system. Hence, experimental measurement of certain crucial parameters is recommended [53,54]. Furthermore, due to limited information availability within the study

area, solely the Zhangjiashan hydrological station, the sole outlet control station, could be utilized to evaluate the accuracy of CMADS at that specific location, resulting in substantial uncertainty. Based on this, this study employed parameters with high sensitivity for tuning in order to diminish uncertainties and enhance efficiency. The hydrological station's control area was fully considered, and parameter conversions were implemented by referencing relevant studies' methodologies to minimize model uncertainties to the greatest extent possible. However, the assessment of model uncertainty was lacking, thus necessitating the inclusion of uncertainty analysis as the subsequent phase of this study [55,56].

(ii) The impacts of climate and land-use change on runoff in the Jing River Basin were evaluated by the validated CMADS+SWAT model. However, despite considering four climate scenarios and four land-use scenarios individually through a comparative analysis, the interconnectedness between climate and land-use changes was overlooked. Climate change not only influenced the growth conditions of crops and natural vegetation, but also triggered responses in the growth of these entities, resulting in a complex and variable interactive relationship between the two [1,57]. To address the intricate physical mechanisms linking climate and land-use, it becomes crucial to develop a robust quantitative model that can uncover the interdependencies between these two factors. Consequently, in future investigations, the inclusion of the CMIP6 model for climate and land-use change analysis will be essential in order to further elucidate the intricate interactions between these aspects.

5. Conclusions

A comparative analysis of precipitation, maximum/minimum temperature between reanalyzed data (CFSR, CMADS) and observation data (OBS), and their spatial distribution both annually and intra-annually was conducted to simulate, validate, and analyze the impacts of climate and land-use change on runoff in the Jing River Basin using the SWAT model. The primary findings are as follows:

(i) CMADS underestimates annual average temperature and total precipitation, whereas CFSR tends to overestimate these variables. However, CMADS exhibits greater accuracy than CFSR in the spatial distribution of annual average precipitation and maximum/minimum temperature, displaying better concordance with OBS. In terms of statistical indicators, CMADS demonstrates lower relative error and root mean square error than CFSR, with the standard deviation ratio being closer to 1. Consequently, CMADS can be considered a more dependable source of reanalyzed data.

(ii) The CMADS+SWAT and OBS+SWAT models demonstrate exceptional performance in simulating runoff, with R^2 values exceeding 0.80 and *NSE* values surpassing 0.79. Conversely, the simulation outcomes of the CFSR+SWAT model are relatively unsatisfactory, displaying a noticeable underestimation in the peak runoff, primarily attributed to the overestimation of weak precipitation and underestimation of intense precipitation in CFSR. In summary, the CMADS+SWAT model exhibits commendable applicability and reliability in the Jing River Basin, maintaining the accuracy of runoff simulation.

(iii) Basin runoff exhibits a positive correlation with precipitation and a negative correlation with temperature. The impact of precipitation on runoff is more pronounced than that of temperature, highlighting the necessity for early warning and prevention measures against heavy rainstorms to mitigate flood risks. Farmland contributes to increased flow, while grassland and forest land play a role in intercepting runoff within the basin. Notably, forest land exhibits stronger interception intensity. Adjusting land-use types and spatial arrangements can effectively prevent flooding incidents. The integrated change results in a decrease of 1.24 m^3/s (I_2) in average annual runoff, with climate change accounting for a reduction of 1.12 m^3/s (I_3) and land-use change contributing to a decrease of 0.12 m^3/s (I_4). The impact of climate change is more significant than that of land0use change, but the role of land-use planning cannot be ignored. Effective land-use planning plays a vital role in addressing the hydrological impact of climate change, particularly its adverse effects.

Author Contributions: The writing, original draft preparation, and data analysis were performed by B.D. The conceptualization, reviewing and editing of the writing, supervision, project administration, and acquisition of funding were carried out by L.W. The manuscript's writing was improved by B.R., L.X. and S.L. All authors have read and agreed to the published version of the manuscript.

Funding: This research was funded by the National Natural Science Foundation of China, grant number 52070158; the National Natural Science Foundation of China, grant number 42277073.

Data Availability Statement: The data that support the findings of this study are available from the corresponding author upon reasonable request.

Conflicts of Interest: The authors declare no conflict of interest.

References

1. Mitiku, A.B.; Meresa, G.A.; Mulu, T.; Woldemichael, A.T. Examining the Impacts of Climate Variabilities and Land Use Change on Hydrological Responses of Awash River Basin, Ethiopia. *HydroResearch* **2023**, *6*, 16–28. [CrossRef]
2. Shrestha, S.; Bhatta, B.; Talchabhadel, R.; Virdis, S.G.P. Integrated Assessment of the Landuse Change and Climate Change Impacts on the Sediment Yield in the Songkhram River Basin, Thailand. *Catena* **2022**, *209*, 105859. [CrossRef]
3. Zhang, Y.; Xia, J.; Yu, J.; Randall, M.; Zhang, Y.; Zhao, T.; Pan, X.; Zhai, X.; Shao, Q. Simulation and Assessment of Urbanization Impacts on Runoff Metrics: Insights from Landuse Changes. *J. Hydrol.* **2018**, *560*, 247–258. [CrossRef]
4. Wang, S.; Ding, Y.; Jiang, F.; Wu, X.; Xue, J. Identifying Hot Spots of Long-Duration Extreme Climate Events in the Northwest Arid Region of China and Implications for Glaciers and Runoff. *Res. Cold Arid Reg.* **2023**, *16*, 347–360. [CrossRef]
5. Xue, P.; Zhang, C.; Wen, Z.; Park, E.; Jakada, H. Climate Variability Impacts on Runoff Projection under Quantile Mapping Bias Correction in the Support CMIP6: An Investigation in Lushi Basin of China. *J. Hydrol.* **2022**, *614*, 128550. [CrossRef]
6. Zokaib, S.; Naser, G.H. A Study on Rainfall, Runoff, and Soil Loss Relations at Different Landuses—A Case in Hilkot Watershed in Pakistan. *Int. J. Sediment Res.* **2012**, *27*, 388–393. [CrossRef]
7. Milly, P.C.D.; Dunne, K.A.; Vecchia, A.V. Global Pattern of Trends in Streamflow and Water Availability in a Changing Climate. *Nature* **2005**, *438*, 347–350. [CrossRef] [PubMed]
8. Gray, L.C.; Zhao, L.; Stillwell, A.S. Impacts of Climate Change on Global Total and Urban Runoff. *J. Hydrol.* **2023**, *620*, 129352. [CrossRef]
9. Li, Y.; Chen, A.; Mao, G.; Chen, P.; Huang, H.; Yang, H.; Wang, Z.; Wang, K.; Chen, H.; Meng, Y.; et al. Multi-Model Analysis of Historical Runoff Changes in the Lancang-Mekong River Basin—Characteristics and Uncertainties. *J. Hydrol.* **2023**, *619*, 129297. [CrossRef]
10. Ni, Y.; Yu, Z.; Lv, X.; Qin, T.; Yan, D.; Zhang, Q.; Ma, L. Spatial Difference Analysis of the Runoff Evolution Attribution in the Yellow River Basin. *J. Hydrol.* **2022**, *612*, 128149. [CrossRef]
11. Wu, L.; Yen, H.; Arnold, J.G.; Ma, X. Is the Correlation between Hydro-Environmental Variables Consistent with Their Own Time Variability Degrees in a Large-Scale Loessial Watershed? *Sci. Total Environ.* **2020**, *722*, 137737. [CrossRef] [PubMed]
12. Zhao, G.; Tian, P.; Mu, X.; Jiao, J.; Wang, F.; Gao, P. Quantifying the Impact of Climate Variability and Human Activities on Streamflow in the Middle Reaches of the Yellow River Basin, China. *J. Hydrol.* **2014**, *519*, 387–398. [CrossRef]
13. Wu, J.; Miao, C.; Zhang, X.; Yang, T.; Duan, Q. Detecting the Quantitative Hydrological Response to Changes in Climate and Human Activities. *Sci. Total Environ.* **2017**, *586*, 328–337. [CrossRef] [PubMed]
14. Gao, X.; Yan, C.; Wang, Y.; Zhao, X.; Zhao, Y.; Sun, M.; Peng, S. Attribution Analysis of Climatic and Multiple Anthropogenic Causes of Runoff Change in the Loess Plateau—A Case-Study of the Jing River Basin. *Land Degrad. Dev.* **2020**, *31*, 1622–1640. [CrossRef]
15. Sharifi, A.; Mirabbasi, R.; Ali Nasr-Esfahani, M.; Torabi Haghighi, A.; Fatahi Nafchi, R. Quantifying the Impacts of Anthropogenic Changes and Climate Variability on Runoff Changes in Central Plateau of Iran Using Nine Methods. *J. Hydrol.* **2021**, *603*, 127045. [CrossRef]
16. Colucci, R.R.; Guglielmin, M. Precipitation–Temperature Changes and Evolution of a Small Glacier in the Southeastern European Alps during the Last 90 Years. *Int. J. Climatol.* **2015**, *35*, 2783–2797. [CrossRef]
17. Faurès, J.-M.; Goodrich, D.C.; Woolhiser, D.A.; Sorooshian, S. Impact of Small-Scale Spatial Rainfall Variability on Runoff Modeling. *J. Hydrol.* **1995**, *173*, 309–326. [CrossRef]
18. Golian, S.; Moazami, S.; Kirstetter, P.-E.; Hong, Y. Evaluating the Performance of Merged Multi-Satellite Precipitation Products over a Complex Terrain. *Water Resour. Manag.* **2015**, *29*, 4885–4901. [CrossRef]
19. Wang, T.; Li, Z.; Ma, Z.; Gao, Z.; Tang, G. Diverging Identifications of Extreme Precipitation Events from Satellite Observations and Reanalysis Products: A Global Perspective Based on an Object-Tracking Method. *Remote Sens. Environ.* **2023**, *288*, 113490. [CrossRef]
20. Germann, U.; Galli, G.; Boscacci, M.; Bolliger, M. Radar Precipitation Measurement in a Mountainous Region. *Q. J. R. Meteorol. Soc.* **2006**, *132*, 1669–1692. [CrossRef]
21. Li, D.; Christakos, G.; Ding, X.; Wu, J. Adequacy of TRMM Satellite Rainfall Data in Driving the SWAT Modeling of Tiaoxi Catchment (Taihu Lake Basin, China). *J. Hydrol.* **2018**, *556*, 1139–1152. [CrossRef]

22. Meng, X.; Zhang, X.; Yang, M.; Wang, H.; Chen, J.; Pan, Z.; Wu, Y. Application and Evaluation of the China Meteorological Assimilation Driving Datasets for the SWAT Model (CMADS) in Poorly Gauged Regions in Western China. *Water* **2019**, *11*, 2171. [CrossRef]
23. Wang, N.; Liu, W.; Sun, F.; Yao, Z.; Wang, H.; Liu, W. Evaluating Satellite-Based and Reanalysis Precipitation Datasets with Gauge-Observed Data and Hydrological Modeling in the Xihe River Basin, China. *Atmos. Res.* **2020**, *234*, 104746. [CrossRef]
24. Ma, D.; Xu, Y.-P.; Gu, H.; Zhu, Q.; Sun, Z.; Xuan, W. Role of Satellite and Reanalysis Precipitation Products in Streamflow and Sediment Modeling over a Typical Alpine and Gorge Region in Southwest China. *Sci. Total Environ.* **2019**, *685*, 934–950. [CrossRef]
25. Tan, M.L.; Gassman, P.W.; Liang, J.; Haywood, J.M. A Review of Alternative Climate Products for SWAT Modelling: Sources, Assessment and Future Directions. *Sci. Total Environ.* **2021**, *795*, 148915. [CrossRef]
26. Worqlul, A.W.; Yen, H.; Collick, A.S.; Tilahun, S.A.; Langan, S.; Steenhuis, T.S. Evaluation of CFSR, TMPA 3B42 and Ground-Based Rainfall Data as Input for Hydrological Models, in Data-Scarce Regions: The Upper Blue Nile Basin, Ethiopia. *Catena* **2017**, *152*, 242–251. [CrossRef]
27. Yu, Z.; Wu, J.; Chen, X. An Approach to Revising the Climate Forecast System Reanalysis Rainfall Data in a Sparsely-Gauged Mountain Basin. *Atmos. Res.* **2019**, *220*, 194–205. [CrossRef]
28. Bai, J.; Zhou, Z.; Li, J.; Liu, T.; Zhu, Q.; Zheng, T. Predicting Soil Conservation Service in the Jinghe River Basin under Climate Change. *J. Hydrol.* **2022**, *615*, 128646. [CrossRef]
29. Liu, S.; Huang, S.; Xie, Y.; Leng, G.; Huang, Q.; Wang, L.; Xue, Q. Spatial-Temporal Changes of Rainfall Erosivity in the Loess Plateau, China: Changing Patterns, Causes and Implications. *Catena* **2018**, *166*, 279–289. [CrossRef]
30. Jin, F.; Yang, W.; Fu, J.; Li, Z. Effects of Vegetation and Climate on the Changes of Soil Erosion in the Loess Plateau of China. *Sci. Total Environ.* **2021**, *773*, 145514. [CrossRef]
31. Wang, B.; Wang, C.; Jia, B.; Fu, X. Spatial Variation of Event-Based Suspended Sediment Dynamics in the Middle Yellow River Basin, China. *Geomorphology* **2022**, *401*, 108115. [CrossRef]
32. Yan, X.; Sun, J.; Huang, Y.; Xia, Y.; Wang, Z.; Li, Z. Detecting and Attributing the Changes in Baseflow in China's Loess Plateau. *J. Hydrol.* **2023**, *617*, 128957. [CrossRef]
33. Zheng, H.; Miao, C.; Zhang, G.; Li, X.; Wang, S.; Wu, J.; Gou, J. Is the Runoff Coefficient Increasing or Decreasing after Ecological Restoration on China's Loess Plateau? *Int. Soil Water Conserv. Res.* **2021**, *9*, 333–343. [CrossRef]
34. Li, Z.; Wang, Y.; Zhang, H.; Chang, J.; Yu, Y. Runoff Response to Changing Environment in Loess Plateau, China: Implications of the Influence of Climate, Land Use/Land Cover, and Water Withdrawal Changes. *J. Hydrol.* **2022**, *613*, 128458. [CrossRef]
35. Hutchinson, M.F.; McKenney, D.W.; Lawrence, K.; Pedlar, J.H.; Hopkinson, R.F.; Milewska, E.; Papadopol, P. Development and Testing of Canada-Wide Interpolated Spatial Models of Daily Minimum–Maximum Temperature and Precipitation for 1961–2003. *J. Appl. Meteorol. Climatol.* **2009**, *48*, 725–741. [CrossRef]
36. Hutchinson, M.F.; Gessler, P. Splines-More Than Just a Smooth Interpolator. *Geoderma* **1994**, *62*, 45–67. [CrossRef]
37. Liang, X.; Guan, Q.; Clarke, K.C.; Liu, S.; Wang, B.; Yao, Y. Understanding the Drivers of Sustainable Land Expansion Using a Patch-Generating Land Use Simulation (PLUS) Model: A Case Study in Wuhan, China. *Comput. Environ. Urban Syst.* **2021**, *85*, 101569. [CrossRef]
38. Abbaspour, K.C.; Rouholahnejad, E.; Vaghefi, S.; Srinivasan, R.; Yang, H.; Kløve, B. A Continental-Scale Hydrology and Water Quality Model for Europe: Calibration and Uncertainty of a High-Resolution Large-Scale SWAT Model. *J. Hydrol.* **2015**, *524*, 733–752. [CrossRef]
39. Moriasi, D.; Arnold, J.; Van Liew, M.; Bingner, R.; Harmel, R.D.; Veith, T. Model Evaluation Guidelines for Systematic Quantification of Accuracy in Watershed Simulations. *Trans. ASABE* **2007**, *50*, 885–900. [CrossRef]
40. Ning, T.; Li, Z.; Liu, W. Separating the Impacts of Climate Change and Land Surface Alteration on Runoff Reduction in the Jing River Catchment of China. *Catena* **2016**, *147*, 80–86. [CrossRef]
41. Zhao, X.; Fang, K.; Chen, F.; Martín, H.; Roig, F.A. Reconstructed Jing River Streamflow from Western China: A 399-Year Perspective for Hydrological Changes in the Loess Plateau. *J. Hydrol.* **2023**, *621*, 129573. [CrossRef]
42. Knoche, M.; Fischer, C.; Pohl, E.; Krause, P.; Merz, R. Combined Uncertainty of Hydrological Model Complexity and Satellite-Based Forcing Data Evaluated in Two Data-Scarce Semi-Arid Catchments in Ethiopia. *J. Hydrol.* **2014**, *519*, 2049–2066. [CrossRef]
43. Shaowei, N.; Jie, W.; Juliang, J.; Xiaoyan, X.; Yuliang, Z.; Fan, S.; Linlin, Z. Comprehensive Evaluation of Satellite-Derived Precipitation Products Considering Spatial Distribution Difference of Daily Precipitation over Eastern China. *J. Hydrol. Reg. Stud.* **2022**, *44*, 101242. [CrossRef]
44. Weinman, J.A.; Guetter, P.J. Determination of Rainfall Distributions from Microwave Radiation Measured by the Nimbus 6 ESMR. *J. Appl. Meteorol. Climatol.* **1977**, *16*, 437–442. [CrossRef]
45. Lyu, J.; Yin, S.; Sun, Y.; Wang, K.; Luo, P.; Meng, X. Flood Runoff Simulation under Changing Environment, Based on Multiple Satellite Data in the Jinghe River Basin of the Loess Plateau, China. *Remote Sens.* **2023**, *15*, 550. [CrossRef]
46. Ajaaj, A.; Mishra, A.; Khan, A. Evaluation of Satellite and Gauge-Based Precipitation Products through Hydrologic Simulation in Tigris River Basin under Data-Scarce Environment. *J. Hydrol. Eng.* **2019**, *24*, 05018033. [CrossRef]
47. Lv, A.; Qi, S.; Wang, G. Multi-Model Driven by Diverse Precipitation Datasets Increases Confidence in Identifying Dominant Factors for Runoff Change in a Subbasin of the Qaidam Basin of China. *Sci. Total Environ.* **2022**, *802*, 149831. [CrossRef]
48. Wang, Z.; Xu, M.; Liu, X.; Singh, D.K.; Fu, X. Quantifying the Impact of Climate Change and Anthropogenic Activities on Runoff and Sediment Load Reduction in a Typical Loess Plateau Watershed. *J. Hydrol. Reg. Stud.* **2022**, *39*, 100992. [CrossRef]

49. Yang, L.; Zhao, G.; Tian, P.; Mu, X.; Tian, X.; Feng, J.; Bai, Y. Runoff Changes in the Major River Basins of China and Their Responses to Potential Driving Forces. *J. Hydrol.* **2022**, *607*, 127536. [CrossRef]
50. Wu, L.; Liu, X.; Yang, Z.; Yu, Y.; Ma, X. Is Climate Dominating the Spatiotemporal Patterns of Water Yield? *Water Resour. Manag.* **2022**, *37*, 321–339. [CrossRef]
51. Eini, M.R.; Rahmati, A.; Piniewski, M. Hydrological Application and Accuracy Evaluation of PERSIANN Satellite-Based Precipitation Estimates over a Humid Continental Climate Catchment. *J. Hydrol. Reg. Stud.* **2022**, *41*, 101109. [CrossRef]
52. Wei, C.; Dong, X.; Ma, Y.; Gou, J.; Li, L.; Bo, H.; Yu, D.; Su, B. Applicability Comparison of Various Precipitation Products of Long-Term Hydrological Simulations and Their Impact on Parameter Sensitivity. *J. Hydrol.* **2023**, *618*, 129187. [CrossRef]
53. Dash, S.S.; Sahoo, B.; Raghuwanshi, N.S. How Reliable Are the Evapotranspiration Estimates by Soil and Water Assessment Tool (SWAT) and Variable Infiltration Capacity (VIC) Models for Catchment-Scale Drought Assessment and Irrigation Planning? *J. Hydrol.* **2021**, *592*, 125838. [CrossRef]
54. Jeyrani, F.; Morid, S.; Srinivasan, R. Assessing Basin Blue–Green Available Water Components under Different Management and Climate Scenarios Using SWAT. *Agric. Water Manag.* **2021**, *256*, 107074. [CrossRef]
55. Song, Y.H.; Chung, E.-S.; Shahid, S. Differences in Extremes and Uncertainties in Future Runoff Simulations Using SWAT and LSTM for SSP Scenarios. *Sci. Total Environ.* **2022**, *838*, 156162. [CrossRef]
56. Sun, G.; Wei, X.; Hao, L.; Sanchis, M.G.; Hou, Y.; Yousefpour, R.; Tang, R.; Zhang, Z. Forest Hydrology Modeling Tools for Watershed Management: A Review. *For. Ecol. Manag.* **2023**, *530*, 120755. [CrossRef]
57. Faye, B.; Webber, H.; Gaiser, T.; Müller, C.; Zhang, Y.; Stella, T.; Latka, C.; Reckling, M.; Heckelei, T.; Helming, K.; et al. Climate Change Impacts on European Arable Crop Yields: Sensitivity to Assumptions about Rotations and Residue Management. *Eur. J. Agron.* **2023**, *142*, 126670. [CrossRef]